8.4 **FALL VELOCITY AND AXIAL RATIO OF SNOWFLAKES**

Raphael Schefold*, Björn Baschek, Marc Wüest, and Eszter Barthazy
Institute for Atmospheric and Climate Science, ETH, 8093 Zürich Switzerland

1 INTRODUCTION

The properties of snowflakes such as their size distribution, fall velocity or axial ratio are important for several purposes. The knowledge of accurate fall velocities, e.g., can be used to calculate aggregation rates in modelling precipitation processes. The size distribution and especially the axial ratios provide information for the interpretation of returned radar power, in particular of polarized radar (Vivekandan, 1993, Fabry, 1999).

Except for some in situ techniques, where snowflakes are captured and examined, optical techniques are the choice when snowflakes are to be investigated. However, accurate experimental observations of size distributions, fall velocities and axial ratios with description of the true spread of each property (e.g. within a size class) are scarce due to either the limited number of observed snowflakes, or to the limitations of the observations techniques (Locatelli, 1974, Zikmunda, 1972).

To overcome these limitations, an optical disdrometer was developed at the ETH Zurich. The instrument is capable to measure several properties like the real time-dependent size distribution in the range of 0.15 - 70 mm or axis ratios and fall velocities of single hydrometeors.

This optical disdrometer is used in ongoing field campaigns (Mt. Rigi and Mt. Uetli, Switzerland) to collect snowflake data of different crystal types. One snowfall event of a few hours can yield data of several tens of thousands of snowflakes. In addition, ice crystals are replicated (Formvar) regularly with time intervals of about 10 minutes to determine their habit and riming degree.

The studies show on a statistical base the dependency of the fall velocity and the axial ratio on the size of the snowflake, but also on the type of snow (crystal type, riming degree).

2 SETUP

Two mountains – the Mount Rigi and Mount Uetli – were chosen as measuring sites for this analysis, which have a steep rising front pointing towards the lowlands and the main weather direction. The setup, as seen in Fig. 1, is identical at both mountains and is split up in two locations – one at the bottom and one close to the top. The steepness of the mountains allows to measure variables on different height levels at similar horizontal position.

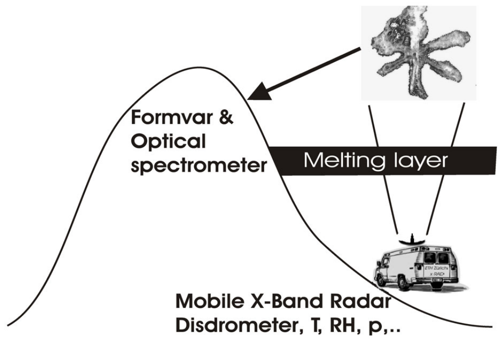

Fig. 1: *Schematic drawing of the setup with two locations, one at the bottom and the second close to the top of the respective mountains.*

At the bottom station is a vertically pointing x-band Radar used, which is described in Baschek, 2002. On the top station the optical spectrometer is used, which is described briefly in the next section. A more detailed description can be found in Barthazy, 2001. In addition, Formvar probes (Schaefer, 1956) were taken at the top station to determine ice crystal types and riming degree.

3 OPTICAL SPECTROMETER

A light source is producing a beam of uniform light directed towards an electronic line scan camera. The optical path of the beam is shielded by a rectangular tube except for a gap of 108.5 mm length near the light source. Precipitation particles falling through the light beam in this gap cast a shadow, which is measured by the line scan camera. The camera is sensitive in two horizontal planes having a vertical distance of 9.45 (±0.55) mm. The length of these measuring planes is given by the dimension of the gap of the housing, the width is given by the dimension of the line scan sensors in the camera and was

* Corresponding author's address: Institute for Atmospheric and Climate Science, ETH Hönggerberg HPP, CH-8093 Zürich, email: schefold@atmos.umnw.ethz.ch

determined to be 76.75 (±4.25) mm. A top and a side view of the sensor unit are shown in Fig. 2.

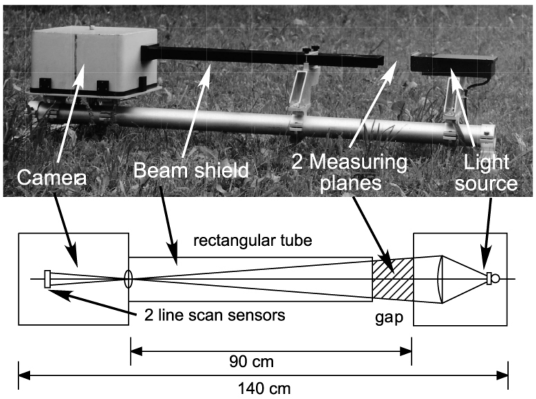

Fig. 2: *Side and top view of the sensor unit.*

4 MATCHING SOFTWARE

Due to the two scan lines every particle is recorded twice. To find the fall velocity of the particle, the two images of the particle have to be matched. We describe now further improvements of the matching software compared to the version described in Barthazy, 2001.

The main idea of the matching process is to compare, within a certain time frame, every image of a particle taken in the upper line scan with every image taken in the lower line scan. Now, not only the shape of the images is compared. In addition, a list is carried on including the horizontal movement of the last ten *already matched* particles. Therefore, an average horizontal movement is also known. The horizontal movement of each potential couple is compared with the average value of that list. If the variation is bigger than a certain cut-off value a match of that potential couple is forbidden.

Interrelated with the matching problem is another new task of the program, which is about the reshaping of the images. There are two cases:

(a) Due to the constant scan rate the shape of the image of a particle does not need to have the shape of the particle itself, e.g. the higher the fall speed of a particle is the less times it will be scanned and the image will be compressed vertically. Similarly, a small fall speed will result in vertically stretched images due to more scans of the particle. We may call this effect "stretching due to velocity".

(b) The other effect has its reason in the horizontal movement of particles in the measuring area, e.g. due to horizontal wind. If the movement of the particle has a component parallel to the line scan cameras, then the shadowed area will shift from scan to scan. The resulting image of the particle will be sheared. We may call this effect "shearing due to horizontal movement". Normally both effects, the stretching and the shearing, cumulate on each particle.

The program "reshapes" the particles after it matched the images from the two light beams in the following way:

Stretching: Images of fast particles appear vertically compressed, those of slow falling particles elongated. The fall velocity threshold is at 1.461 ms^{-1}, at which the images are not distorted vertically. This threshold value is given by the scan frequency and the distance between the two measuring planes. If the fall velocity is known, the vertical distortion of the image can easily be corrected.

Shearing: Horizontally moving particles produce sheared images due to the shift of the particle between scans. The program shifts back each line under the assumption that the shift between scan lines is a linear part of the complete shift of the particle between the left and right frame of the block.

The last task of the matching program is then to print out (a) the geometrical information of every matched particle like sketched in Fig. 3, (b) the horizontal and vertical movement information and (c) flags, which indicate, how “secure” the chosen match is.

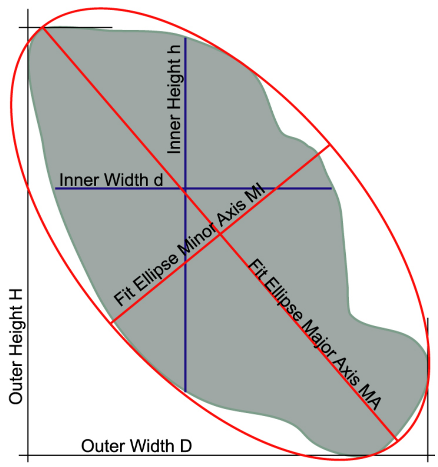

Fig. 3: *Definition of the calculated dimensions of a particle*

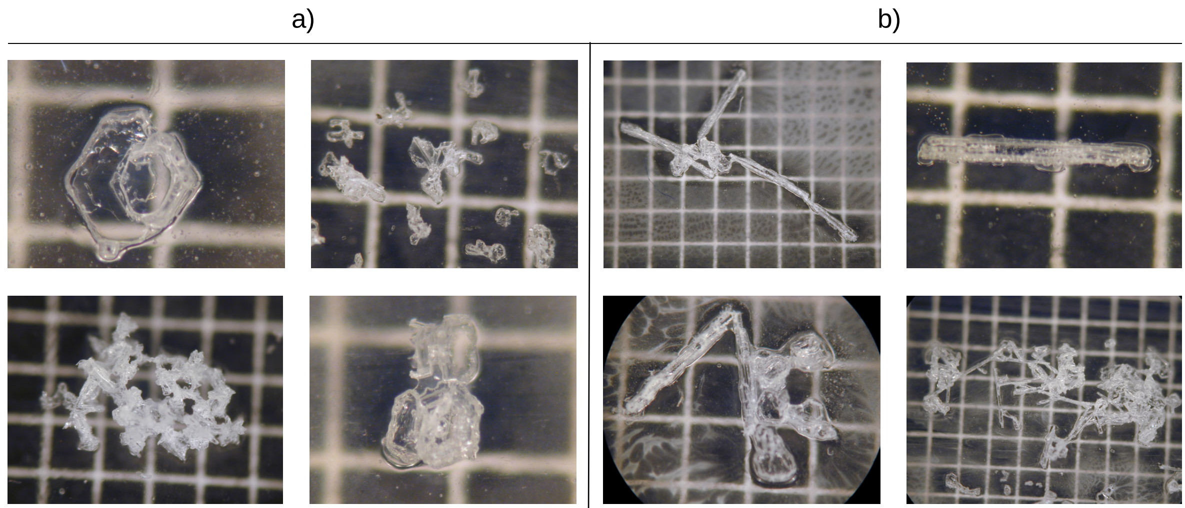

Fig. 4: *Formvar replica of unrimed (class 0) snow crystals. The grid size is 1 mm. a) solid plates and aggregates of them at 14:40 – 14:50, b) needles and aggregates of them at 17:30 – 17:40*

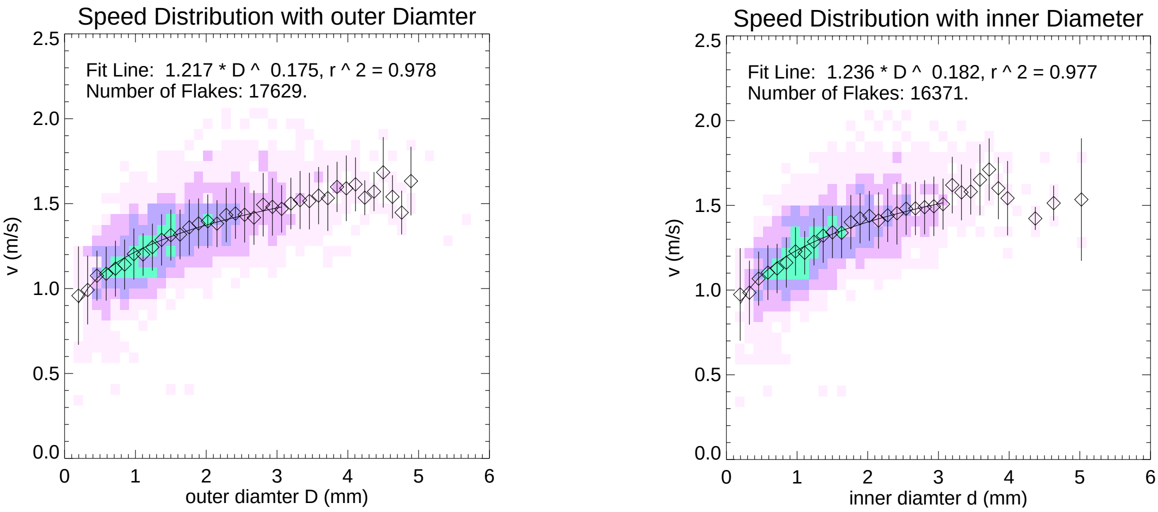

Fig. 5: *Speed distribution of solid thick plates in aggregation or irregular crystals of planar type at 14:40 – 14:50. For a legend, see Fig. 12.*

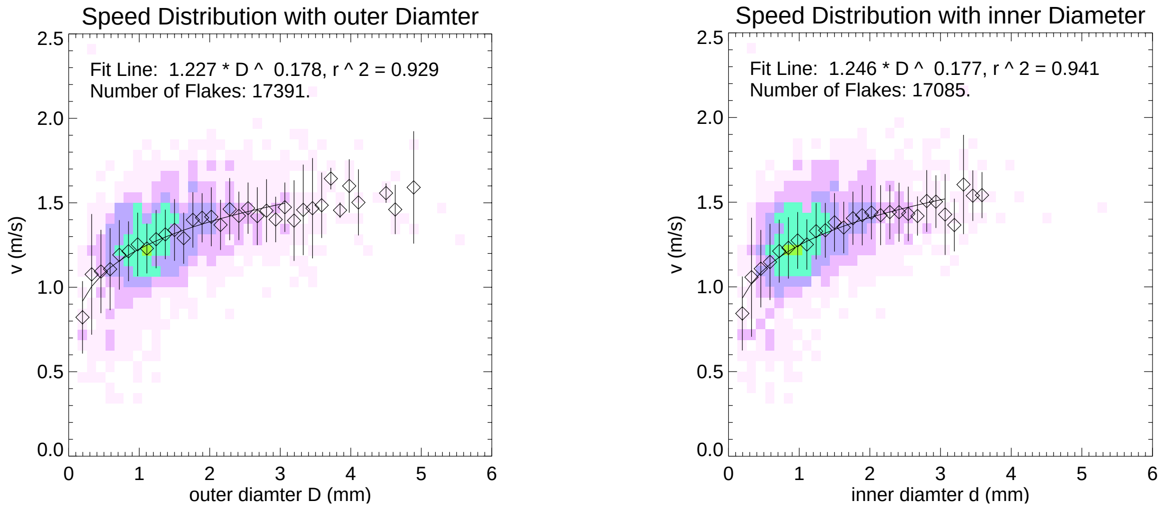

Fig. 6: *Speed distribution of crystals and aggregates of needles and irregular crystals of planar type at 17:30 – 17:40.*

5 FIRST RESULTS

5.1 Different crystal types I

Several case studies have been taking place in winter season 2001/2002. On 6 February 2002 a stratiform case was observed on Mt. Rigi (Baschek, 2002). Formvar probes show two types of particles which were taken at two different times (Fig. 4). These two times were chosen, at which a crystal identification could be made (Magono, 1966). At the first time, solid thick plates in combination or aggregation or irregular crystals of planar type were observed (these particles are referred to as type P particles hereafter), whereas at the second time, single crystals and small to medium aggregates of needles and irregular crystals of planar type (hereafter type N) were observed. In Figs. 5 and 6, particle speed distributions are shown. For a legend, see Fig. 12. The Figs. 5a and 6a describe distributions, where the particles are sorted in size classes according to their outer diameter. In Figs. 5b and 6b the particles are sorted according to their inner diameter (compare also Fig. 3). The average speed value and the standard deviation for each size class is also shown in the plots. The fist size class (0 - 150 µm) in unoccupied. A curve of the form $v = a \cdot D^b$ is fitted to the average speed values in the diameter range of 0.150 - 3 mm, where the main occupation of the size classes happens. All four fits in Figs. 5 and 6 describe very similar curves. r^2 reaches good values. Two conclusions are made out of this observation:

Particle Diameter: The occupations of the bins, gained from inner and outer diameter, are similar for one particle type. Therefore, optical measurements of particle speed distributions seem to be independent of the kind of the observed particle width.

Particle Fall speeds: In the range of 300 µm to 3 mm, the average values of the fall speeds are similar. It appears that the particle fall speeds depend most on the irregular crystals, which is occurring in both particle types N and P.

In Fig. 7, axis ratios for both particle types are shown, where the outer diameter is used now to sort the particles in size classes. For comparison purposes a curve of the form $a \cdot D^b$ is fitted to the average values in the diameter range of 150 µm - 3 mm. The fit parameter b is -0.113 for the P type and -0.180 for the N type particles. Therefore, the axis ratio of the P particle type is less depending on the diameter, whereas the axis ratio of the N particle type varies more with the diameter. Hence, type N particles fall in a slightly more oriented manner than type P particles.

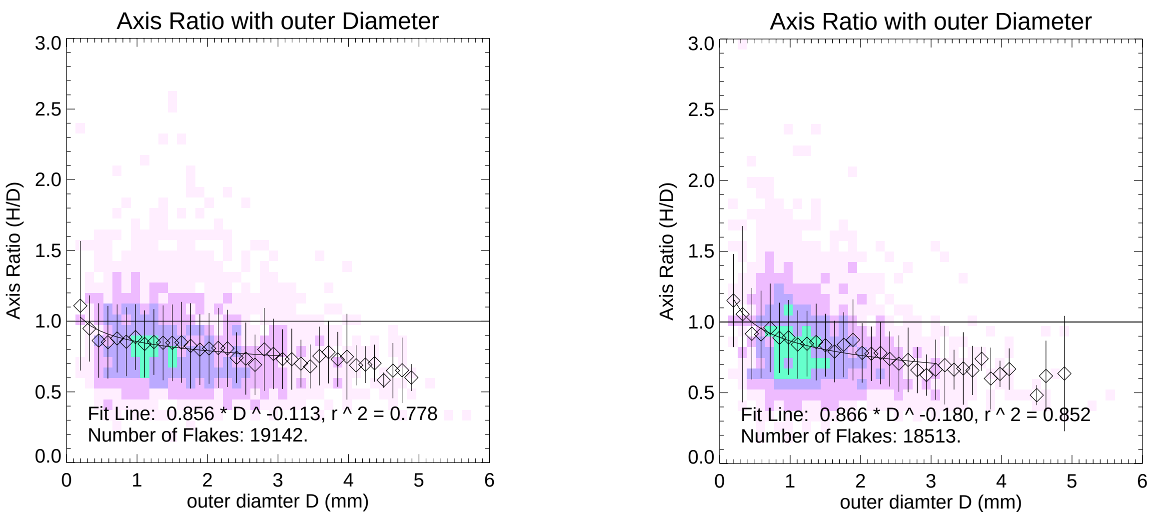

Fig. 7: *Axis ratios of measured aggregates. Left: solid thick plates in combination or aggregation or irregular crystals of planar type, right: single crystals and small to medium aggregates of needles and irregular crystals of planar type.*

a) b)

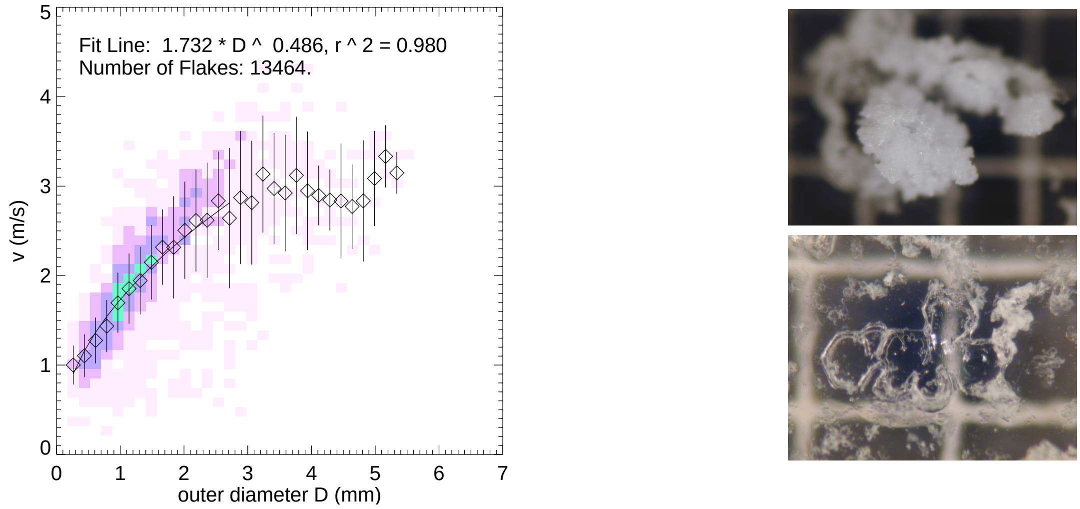

Fig. 8: *Speed distribution and Formvar replica of particles at 10:30 – 10:50. The grid size is 1 mm. Hexagonal crystals and aggregates, some of them rimed and some of them* with sectorlike or broad branches.

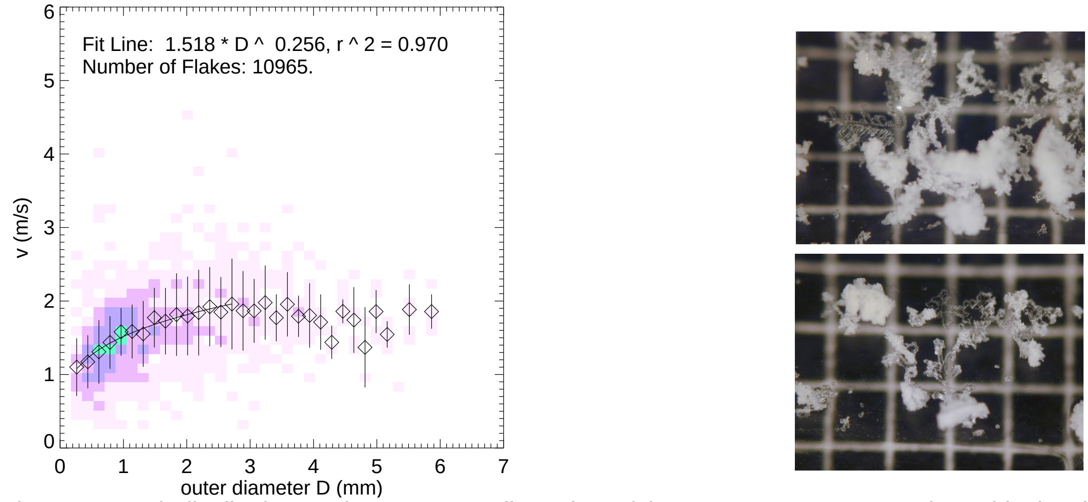

Fig. 9: *Speed distribution and Formvar replica of particles at 10:50 – 11:10. The grid size is 1 mm. Crystals and aggregates, some of them rimed and/or* with dendritic extensions.

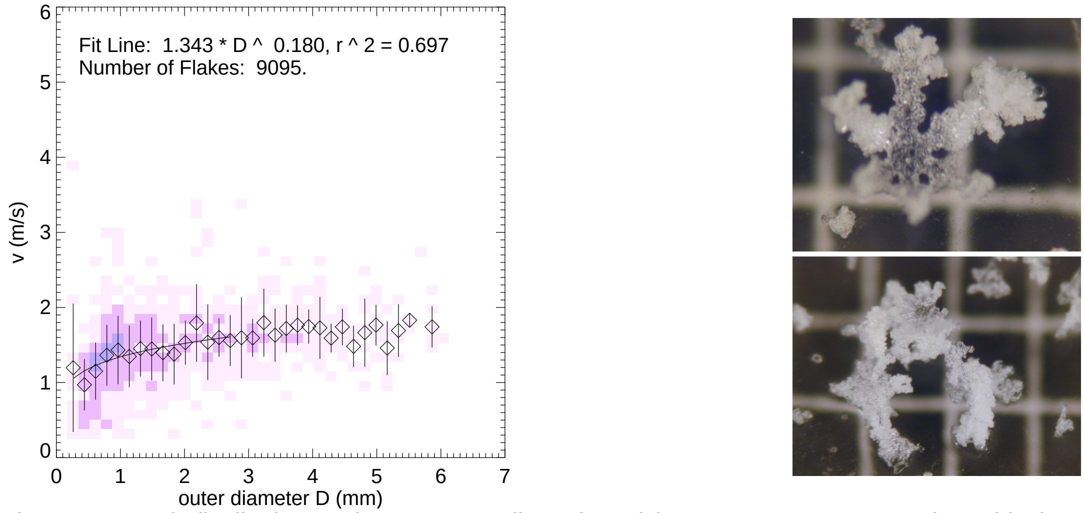

Fig. 10: *Speed distribution and Formvar replica of particles at 11:10 – 11:30. The grid size is 1 mm. Crystals and aggregates, some of them rimed and* with mostly dendritic extensions.

5.2 Different Crystal Type II

On 21 February 2002 another stratiform case was observed on Mt. Rigi. Formvar probes show different types of crystals and aggregates which were taken at several times. A crystal identification (Magono, 1966) was made on three times (Figs. 8a, 9a, and 10a). Some of the crystals and aggregates were slightly rimed (Mosimann, 1994). In Fig. 8a, most crystals have a hexagonal structure, where some of them have sectorlike and broad branches (hereafter referred to as type A). In Fig. 9a dendritic extensions happen (type B). In Fig. 10a most of the extensions are dendritic (type C). Figs. 8a, 9a and 10a show the corresponding speed distributions, where a curve of the form $v = a \cdot D^b$ is fitted to the average speed values in the diameter range of 0.150 - 2.7 mm. These fit curves are shown in Fig. 11. It is a clear dependence on the type of the particles recognizable. The type A particles have the highest, whereas the type C particles have the lowest fall speed. A possible explanation for the difference in the measured fall speeds for the different types is the much lower density of the dendritic type C particles compared to the type A particles.

6 CONCLUSION & OUTLOOK

The most general result of this ongoing work is, that the measurement of fall speeds seems to be insensitive on the chosen particle diameter (inner or outer particle width). Other results emphasise well known interrelations. Now, new parameters of hydrometeors, such as their fall velocity and axial ratio are now available which could be measured up to now only for some selected snowflakes but not for a whole precipitation event. Future work will therefore introduce better precision into in-situ measurements of precipitation particles.

7 ACKNOWLEDGMENTS

Thanks are due to Tobias Grimbacher, a Ph.D. colleague, for help with measurements and weather forecasting and Peter Eltz, who is doing his diploma thesis in our group, for help with measurements and programming.

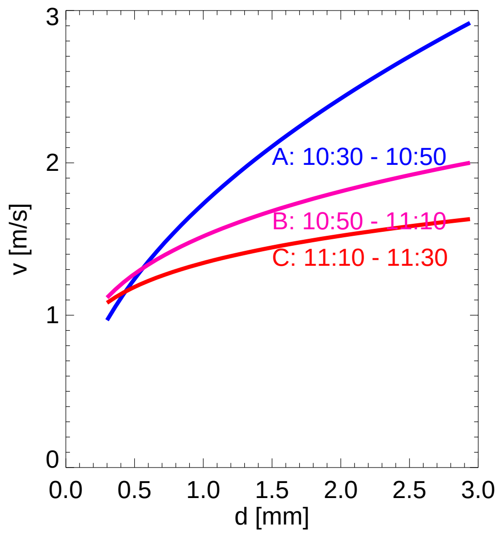

Fig.11: *Fit curves of fall speeds of three different particle types on three different times.*

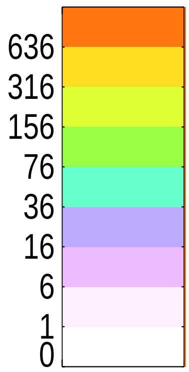

Fig. 12: *Legend for colour plots. Each colour represents a range representing the occupation of a bin.*

8 REFERENCES

Baschek, B. R. et al, 2002. Influence of embedded convection on microphiysics of precipitation. 11th Conference on Cloud Physics, AMS, Ogden (2002).

Barthazy, E, and R. Schefold, 2001. A new ground-based optical instrument to measure snowflakes. 30th International Conference of Radar Meteorology, AMS, München (2001).

Fabry, F., and W. Szyrmer. 1999. Modeling of the melting Layer. Part II: Electromagnetic. *J. Atmos. Sci*., **56**, 3593-3600.

Locatelli, J. D., and P. V. Hobbs, 1974. Fall speeds and masses of solid precipitation particles. *J. Geophys. Res*., **79**, 2185.

Magono, C, and C. W. Lee, 1966. Meteorological classification of natural snow crystals. Pp. 321-355. *J. Fac. Sci.*, Vol. II, No. 4 of *VII*. Hokkaido University, Japan.

Mosimann, L, E. Weingartner, and A. Waldvogel, 1994. An Analysis of accreted drop sizes and mass on rimed snow crystals. *J. Atmos. Sci.,* **51***,* 1548-1558

Schaefer, V.J. 1956. The preparation of snow crystal replicas. *Weatherwise,* **93**, 239-240

Vivekanandan, J., R. Raghaven and V.N. Bringi, 1993: Polarimetric radar modeling of mixtures of precipitation particles. *IEEE Trans.on Geoscience and Remote Sensing*, **31**, No. 5, 1017-1030.

Zikmunda, J, 1972. Fall velocities of spatial crystals and aggregates. *J. Atmos. Sci*., **29**, 1511.